communications earth & environment

Article

https://doi.org/10.1038/s43247-024-01497-2

Three-dimensional analysis reveals diverse heat wave types in Europe

Ondřej Lhotka [1,2] ✉ & Jan Kyselý[1,3]

Heat waves are among the most studied atmospheric hazards but commonly investigated near-surface temperature patterns provide only limited insight into their complex structure. Here we propose and evaluate a novel approach to the analysis of heat waves as three-dimensional (3D) phenomena, employing the ERA5 reanalysis in three European regions during 1979–2022. Four types of heat waves based on their vertical cross sections of temperature anomalies are introduced: near-surface, lower-tropospheric, higher-tropospheric, and omnipresent. The individual heat wave types differ in length, predominant occurrence within summer, and soil moisture preconditioning. While near-surface heat waves may persist for more than 2 weeks, those located mainly in higher troposphere are shortest (5 days at most). This demonstrates that warm advection must be accompanied by a downward propagation of positive temperature anomalies through air subsidence and diabatic heating to maintain long-lasting heat waves. We also show that soil-moisture preconditioning is crucial for near-surface heat waves only, thus pointing to different driving mechanisms for the individual 3D heat wave types.

Heat waves are attracting growing attention[1] due to recent unprecedented events in many regions[2]. The term heat dome[3] refers to an excessively warm area beneath a stationary and persistent summertime anticyclone, emphasizing the three-dimensional (3D) nature of heat waves. The most notable recent events include the 2021 Western North American heat wave[4], the 2022 heat wave in Eastern China[5], and the 2022 Western European heat wave[6]. Even though these and other major heat waves have shattered numerous near-surface temperature records and were related to major societal and environmental losses, the relative contributions of their physical drivers (advective, adiabatic, and diabatic) are still not well understood[7] and only limited knowledge is available about their vertical temperature profiles and 3D structures.

Atmospheric profiling revealed that the 2010 heat wave[8] was characterized not only by excessive heat near the surface but also throughout the lower troposphere in Eastern Europe (up to 4 km at least)[9]. Miralles et al.[10] investigated vertical properties of potential temperature across the lower troposphere under excessively hot conditions during the major 2003 and 2010 European heat waves. Data from atmospheric profiling suggest formations of anomalously deep and warm nocturnal residual layers, storing the heat from one day to the next, upon which it merges again into the diurnal atmospheric boundary layer[11]. Similar results were obtained for the United States, as ref. 12 found deeper diurnal atmospheric boundary layers and warmer nocturnal residual layers during heat waves, compared to non-heat wave days.

The development of the residual layers was linked to soil desiccation[13]. Soil moisture availability has been identified as an important modifier of daily temperature maxima due to a latent/sensible heat flux partitioning[14]. Heat waves were found to be amplified not only by local desiccated soils but also by advection of sensible heat from upwind dry regions[15]. In addition, soil moisture–temperature coupling is not linear—it depends on region-specific thresholds, below which the sensitivity of temperatures to soil moisture availability increases considerably[16]. Soil moisture–temperature coupling is also modified by orography[17] and land cover[18], suggesting complex bi-directional relationships between soil moisture and heat waves in 3D space.

We aimed to advance our understanding of heat waves' 3D structures through more systematic analyses using spatially and vertically coherent data from the ERA5 reanalysis[19] in several European regions. Aiming to reach a more holistic view of heat waves and their 3D patterns, we propose and evaluate heat waves based on their vertical structure in addition to temperature anomaly, duration, and spatial extent.

Results

Heat waves as three-dimensional (3D) phenomena

Heat waves are investigated in three European regions: the British Isles (BI), France (FR), and Middle Europe (ME). These represent the subset of well-established PRUDENCE regions[20], which have been employed extensively within the climate community because of their balance between natural and

[1]Institute of Atmospheric Physics of the Czech Academy of Sciences, Prague, Czech Republic. [2]Global Change Research Institute of the Czech Academy of Sciences, Brno, Czech Republic. [3]Faculty of Environmental Sciences, Czech University of Life Sciences, Prague, Czech Republic.
✉e-mail: ondrej.lhotka@ufa.cas.cz

socioeconomic boundaries[21]; the subset of the PRUDENCE regions was selected to minimize differences in spatial extent, mean altitude, and share of water bodies. We use 2 m temperature data and temperatures at 12 vertical levels (from 850 up to 300 hPa with 50 hPa step) in the period of 44 years from 1979 to 2022 in the extended summer season (months June–September). For a straightforward interpretation of heat waves' 3D structures, three vertical layers are defined: near-surface (2 m temperature), lower troposphere (mean of levels from 850 to 600 hPa), and higher troposphere (550 to 300 hPa mean).

Based on prevailing locations of temperature anomalies above the 95th percentile calculated for each vertical layer combined with spatial and temporal criteria (see Online methods), we classify heat waves into four types: near-surface (HWG), lower-tropospheric (HWL), higher-tropospheric (HWH), and omnipresent (HWO). The individual types differ clearly in their vertical cross sections, which show also temporal development of intensity and spatial extent of regionally averaged positive temperature anomalies (Fig. 1).

HWG are characterized by large positive temperature anomalies (intensity and spatial extent combined) in the near-surface layer (Fig. 1a–c). Although the anomalies may be larger at 850–750 hPa levels (especially in BI), the remainder of the lower troposphere is characterized by small positive temperature anomalies during HWG (which reduces the lower-tropospheric mean). In the higher troposphere, the magnitude and spatial extent of positive temperature anomalies are negligible. This structure resembles a gradual build-up of near-surface excessively hot conditions and deepening of the atmospheric boundary layer through soil moisture feedback loops[18,22], as observed during the European mega-heatwaves[8].

By contrast, near-surface positive temperature anomalies are much weaker for HWL (Fig. 1d–f). Positive temperature anomalies are concentrated in the lower troposphere, hinting a key role of lower-tropospheric warm advection into the given region. A recent example is the June 2019 Western European heat wave, which was related to intense advection of hot air from North Africa across Spain to France[23]. HWH (Fig. 1g–i) are typical for substantial positive temperature anomalies in the higher troposphere, while near-surface anomalies tend to be negligible. The remaining heat wave type, HWO, is characterized by a relatively even distribution of positive temperature anomalies among the layers. These anomalies tend to be more pronounced in the higher troposphere when heat waves start and seemingly propagate downward during their lifespans (Fig. 1j–l). Similar (but less pronounced) behavior can be observed also in the other types.

This pattern is probably related to higher-tropospheric advection into a given region before heat wave conditions develop near the land surface[24]. After this initial phase, the air mass starts descending while undergoing adiabatic warming[25]. The key role of air subsidence has been emphasized recently, as it may be more important than near-surface warm advection in governing large positive temperature anomalies at lower levels[26,27]. Nevertheless, the relative contributions of heat waves' physical drivers vary on regional and global scales[28].

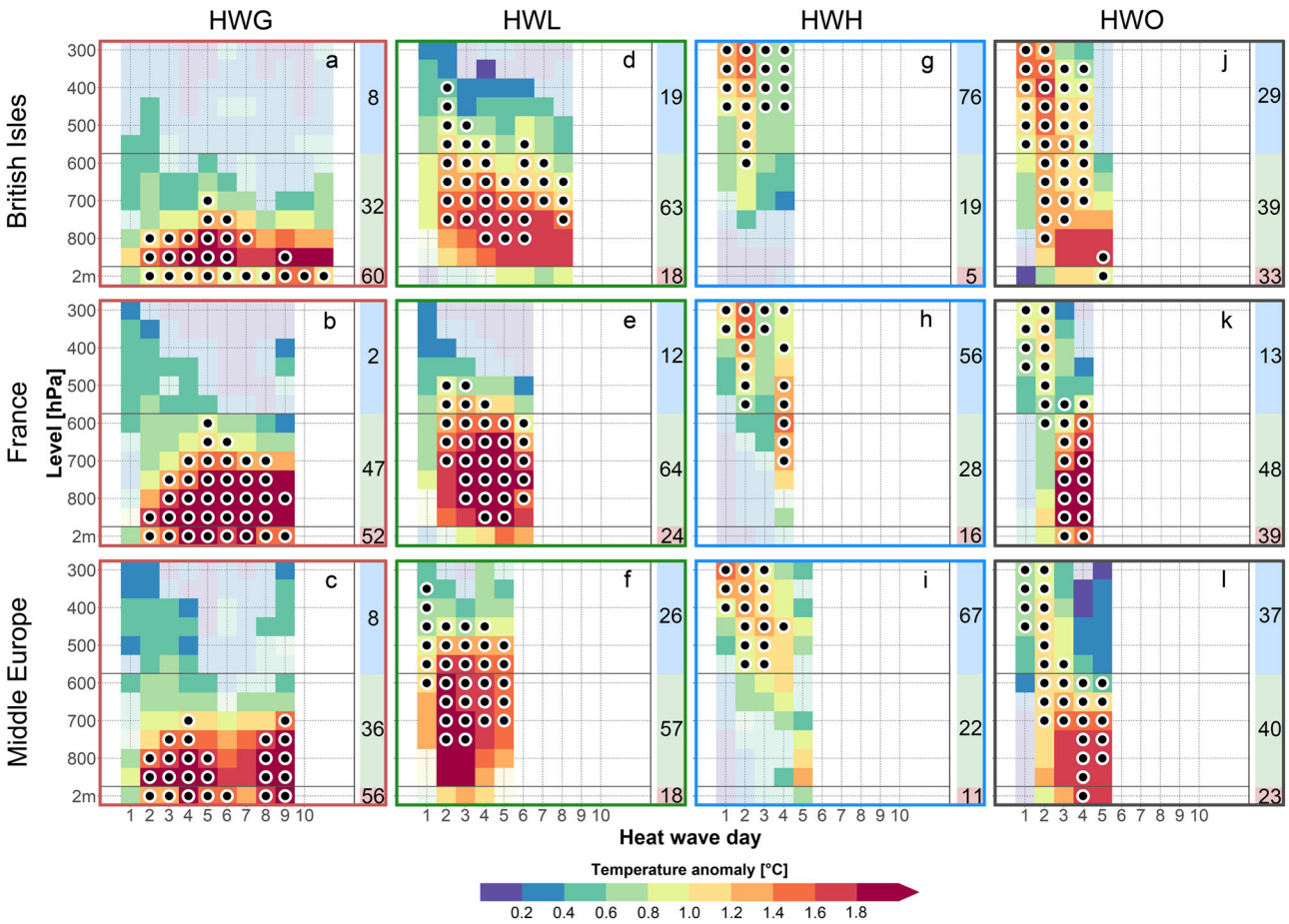

Fig. 1 | Mean cross sections of positive temperature anomalies for the heat wave types. Mean cross sections showing the temporal evolution of regionally averaged temperature anomalies above the 95th percentile of summertime (June–August) daily temperature distribution for individual heat wave types: HWG – near-surface (**a**–**c**), HWL – lower-tropospheric (**d**–**f**), HWH – higher-tropospheric (**g**–**i**), and HWO – omnipresent (**j**–**l**). The plots were cropped on the right when the number of heat waves for a given length dropped below three. Dots indicate days and levels at which positive temperature anomalies occurred in at least 50% of the region, while pale shading represents mean positive temperature anomalies over less than 25% of the domain. Numbers stand for mean proportions [%] of positive temperature anomalies (intensity and spatial extent combined) in near-surface (red), lower troposphere (green), and higher troposphere (blue background) layers.

Temporal characteristics of heat wave types

While the frequencies of all heat wave types are comparable in the three regions, except that there is a lower occurrence of HWO in BI and FR (Fig. 2), we found distinct differences in their duration and timing within the extended summer season. HWG have the largest mean and maximum lengths in all regions and clearly dominates among the longest heat waves (Fig. 2a–c). The maximum length is 15–17 days for HWG in all regions but only 5 days for HWH. Heat waves longer than a week are in more than two-thirds of type HWG, and in BI and ME, 5 out of 6 longest heat waves were classified as HWG (Fig. 2a–c). By contrast, HWH and HWL are the most common among short heat waves, especially in BI and FR. This striking difference in length between HWG and HWH suggests that warm advection at higher tropospheric levels is not sufficient on its own to produce a long-lasting heat wave and must be accompanied by interactions with the boundary layer and land surface, which support heat waves' persistence.

The individual heat wave types differed also in their occurrence within the extended summer season. In BI and FR, kernel density curves of HWG had a marked peak in mid-summer (the second half of July), suggesting stronger influence of diabatic heating (through radiation and surface heat fluxes) compared to the other types (Fig. 2d, e). The occurrence of HWG then drops rapidly, making this type the least frequent in late-summer (the second half of August and September). HWO had a similar pattern but with a less pronounced peak. Within-season occurrences of HWL and HWH were distributed much more evenly, with increasing representation towards the second half of summer, which may be related to warmer Mediterranean waters supporting warm southerly advection in lower or higher troposphere[24]. In the more continental ME climate (Fig. 2f), by contrast, differences in within-season timing between individual heat wave types were less pronounced. In this region, each type had a single peak centered around the turn of July and August, but analogously to BI and FR, HWL and HWH were the types observed most frequently after mid-August.

The exceptional 2003 heat wave[29] remained the most severe in all three regions according to its extremity (a combination of length, temperature anomalies, and spatial extent across layers; see Online methods). Other severe heat waves that struck all three regions are the 2016[30], 2019[23], and the recent 2022[31] events (Table 1). It is notable that the timing of these severe heat waves spanned across the whole extended summer season from June to September. The June 2019 heat wave is classified as HWL (the most frequent type in early summer, Fig. 2d, e); the mid-summer 2003, 2019, and 2022 events are assigned to HWG or HWO types (with an exception for 2003 in BI), and the September 2016 heat wave is classified as HWH. The latter ranked relatively high compared to previous studies[30,32] due to its exceptional positive temperature anomalies in the higher troposphere that cannot be addressed using conventional two-dimensional methods and near-surface data. This event poses a striking example of a late-summer heat wave related to record-breaking values of 500 hPa geopotential heights due to

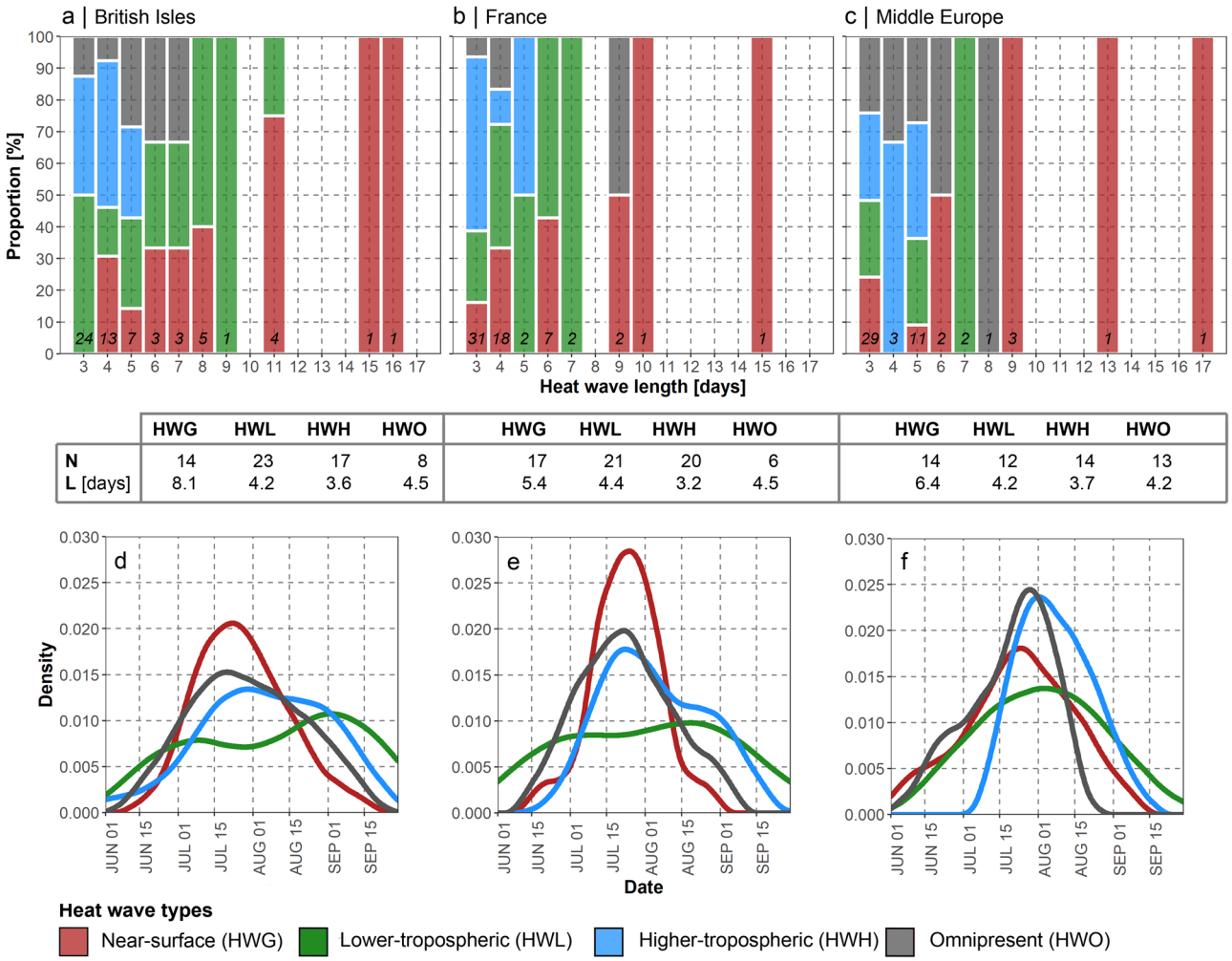

	HWG	HWL	HWH	HWO	HWG	HWL	HWH	HWO	HWG	HWL	HWH	HWO
N	14	23	17	8	17	21	20	6	14	12	14	13
L [days]	8.1	4.2	3.6	4.5	5.4	4.4	3.2	4.5	6.4	4.2	3.7	4.2

Fig. 2 | Lengths and timing within the extended summer season for the heat wave types. Proportions of near-surface (HWG), lower-tropospheric (HWL), higher-tropospheric (HWH), and omnipresent (HWO) types for different heat wave lengths in **a** the British Isles, **b** France, and **c** Middle Europe. The counts of heat waves of a given length are shown in the vertical bars. "*N*" indicates the overall number of heat waves of a given type during 1979–2022, while 'L' stands for their mean length in days. Kernel density curves show the timing of heat wave types within the extended summer season (**d**–**f**).

Table 1 | The most severe heat waves in the British Isles, France, and Middle Europe

British Isles				France				Middle Europe			
Start date	Length	E_{ALL}	Type	Start date	Length	E_{ALL}	Type	Start date	Length	E_{ALL}	Type
04 August 2003	9	22.4	HWL	31 July 2003	15	39.6	HWG	01 August 2003	13	26.7	HWG
22 July 2019	5	18.9	HWO	25 June 2019	6	25.0	HWL	24 June 2019	7	20.9	HWL
01 September 1999	5	13.2	HWO	11 July 2022	9	19.9	HWO	22 July 2019	5	20.3	HWO
10 August 1995	11	13.0	HWG	22 July 2019	4	15.7	HWG	23 July 2018	17	19.5	HWG
17 July 2022	3	12.7	HWL	02 August 2018	6	12.3	HWG	30 June 2015	8	12.2	HWO
09 August 2022	7	12.5	HWO	04 September 2016	4	11.7	HWH	23 August 2016	5	11.6	HWL
24 June 2018	7	11.9	HWL	04 August 2020	9	11.1	HWG	05 September 2016	5	11.2	HWH
05 September 2016	3	11.8	HWH	01 August 1990	4	9.9	HWG	18 July 2022	3	10.2	HWL
07 August 1997	16	11.5	HWG	06 August 1998	6	9.6	HWL	05 August 2020	9	10.1	HWG
27 June 2019	3	11.5	HWL	15 July 2006	10	8.5	HWG	26 July 1983	7	9.8	HWL

Top ten heat waves in individual regions according to their extremity (E_{ALL}; a combination of length, temperature anomalies, and spatial extent across layers, see Online Methods).

high-amplitude Rossby wave packets in Western Europe[30]. The most severe heat waves are visualized in Fig. 3 for FR, and in Supplementary Figs. 1 and 2 for the other regions.

In Supplementary Fig. 3, an example of the spatio-temporal evolution of temperature anomalies and flow characteristics at 500, 850 hPa, and 2 m levels is shown for the recent severe July 2022 heat wave over the British Isles[31] (classified as HWL). This heat wave marked a major milestone in the United Kingdom's climate history, with daily maximum temperatures reaching 40 °C for the first time (on July 19), far exceeding the previous UK record-high temperature of 38.7 °C[33]. Temperatures were record-breaking also in northwestern France and the heat wave was among top 10 according to extremity in all three regions (Table 1). The plots illustrate the development of major positive temperature anomalies at the 850 hPa level (in contrast to much weaker anomalies at 500 hPa). A marked shift of flow direction (from westerly to southerly) occurred between July 17 and 19 at the 500 hPa level, increasing the role of warm advection related to a subtropical high-pressure ridge (Supplementary Fig. 4). The lower-tropospheric warming was supported by air subsidence under anticyclonic conditions.

Links between heat wave types and soil moisture content

As the positive feedback loop between high temperatures and soil desiccation amplifies heat waves[18,22], we investigated links between individual heat wave types and soil moisture (represented by volumetric soil water in the upper layer from ERA5). The temporal development of soil moisture during individual heat waves is plotted in Fig. 4. In all three regions, the vast majority of HWG started when the soil moisture content was below the 25th percentile. HWG are also linked to significant (at 1% level) surface preconditioning on a moderate timescale (periods 14 days long prior to heat waves' onset; Table 2).

In FR (and to a lesser extent in ME), HWG largely contributes to the portfolio of recent severe heat waves (Table 1). In BI, by contrast, just two rather more distant HWG that occurred in 1995 and 1997 are included in Table 1. This discrepancy can be explained by the key role of soil moisture preconditioning for HWG, because the British Isles rarely experienced severe drought in the 2010s, and almost no extreme drought was observed according to the SPEI-12 index[34]. By contrast, in Western and Central Europe, the 2011–2019 period was characterized by approximately 20–30 (5–15) months under severe (extreme) drought conditions[34], thus supporting the contrasting pattern in the occurrence of major HWG in BI compared to the other two regions. This finding is in line with ref. 35, who reported that the majority of the warming summer trend in France is linked to increasing early summer soil moisture deficit.

No heat wave type other than HWG is associated with significant soil moisture preconditioning or systematically lower soil moisture content during its onset throughout the regions (Table 2). Only in ME, HWL and HWO have significantly lower soil moisture content during their onset, but these deficits are less pronounced compared to those of HWG. It is noteworthy that HWL is characterized by the most intense soil desiccation in all regions, despite their shorter lifespan compared to HWG (Table 2). Although this intense drying may be related to relatively wet initial conditions during the HWL onset (compared to HWG; Fig. 4 and Table 2), cross sections of positive temperature anomalies indicate a relatively stable atmospheric stratification or even a presence of lower-tropospheric inversion for HWL (Fig. 1) that suppresses the development of convective precipitation systems[36] and supports soil desiccation.

Discussion and outlook

Our study constitutes a first attempt to systematically investigate heat waves in terms of their 3D structures. We determined differences between individual heat wave types (classified based on their vertical cross sections of temperature anomalies) in their length, timing within the extended summer season, and links to soil moisture content during and prior to their onset. The presented results suggest specific driving mechanisms for individual heat wave types, which may also differ between the early and late stages of their lifespan. Temperature extremes in mid-latitudes are primarily driven by large-scale circulation patterns[37]; the two main factors linked to heat waves in Europe are high-latitude blocking anticyclones and subtropical ridges of high pressure[38].

Both anticyclones and high-pressure ridges are related to anomalies in diabatic heating, air subsidence, and near-surface advection, driving the occurrence of heat waves[39]. Zschenderlein et al.[24] identified varying importance of these processes across European regions—adiabatic warming during air subsidence was found to be more relevant for heat waves' development in Western Europe. In Eastern Europe, by contrast, the role of diabatic heating and near-surface advection is larger. The more important role of surface fluxes in continental climates is probably manifested in a substantially larger share of HWG and HWO types in ME, compared to the maritime climate of BI (where HWL and HWH are dominant).

The HWG type is distinguished from others by significant soil moisture preconditioning. Desiccated soils amplify high-temperature extremes[40] and this coupling was found to be strong during the 2003, 2010, and 2018 heat waves[41]. It should be noted that precipitation observations are not assimilated into the ERA5 reanalysis but produced through large-scale cloud and precipitation schemes and parametrization of convection[19,42]. Therefore, uncertainties in the precipitation-temperature relationship[43] may affect the near-surface layers' temperature and heat wave 3D types, which will be addressed in further studies employing the E-OBS data set[44] for reference precipitation.

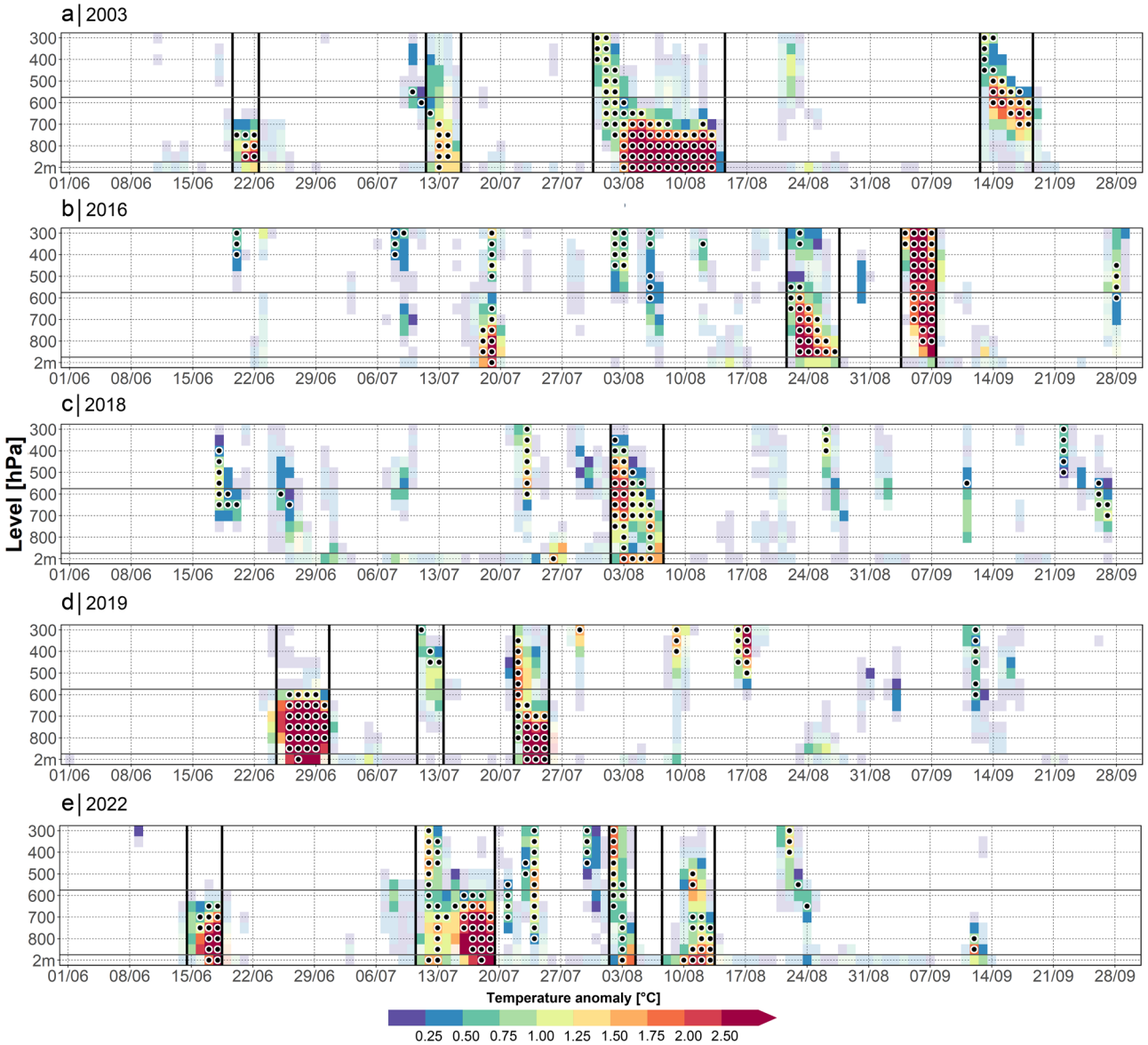

Fig. 3 | Cross sections of positive temperature anomalies in 2003, 2016, 2018, 2019, and 2022. Cross sections of positive temperature anomalies above the 95th percentile of summertime (June–August) daily temperature distribution for years with the most extreme heat waves in the France region; **a** 2003, **b** 2016, **c** 2018, **d** 2019, **e** 2022. Dots indicate those positive temperature anomalies occurring over at least two-thirds of the region, while pale shading represents positive temperature anomalies over less than one-third of the domain (note the difference from Fig. 1). Black vertical lines delimit individual heat waves.

Nevertheless, we argue that considering 3D structures is important for disentangling physical drivers of heat waves, which is one of the current challenges[45] also with respect to improving the credibility of climate change scenarios of heat waves and providing more reliable climate services.

Methods

Data

Temperature data were taken from the ERA5 reanalysis[19]. ERA5 is provided in a global spatial coverage (0.25° longitude–latitude grid) and is available from 1940 to the present in an hourly time step. Daily means (calculated from 24 hourly values) of near-surface (2 m) air temperature (T2M), air temperature at 12 pressure levels from 850 to 300 hPa (50 hPa step), and volumetric soil water (SWVL) in the upper layer (down to 7 cm; over land areas only) were calculated in each grid box. Heat waves were analysed in the 1979–2022 period (considering the onset of the satellite era and related assimilation of those data into ERA5). To provide regionalized heat waves' characteristics, 3 (out of 8) established European regions[20] with similar spatial extent (~$0.6 \times 10^6 \pm 0.1 \times 10^6$ km^2) and mean altitude (~110 ± 50 m a.s.l.) were used: (i) the British Isles (10W–2E, 50–59 N), (ii) France (5W–5E, 44–50 N), and (iii) Middle Europe (2–16E, 48–55 N; Supplementary Fig. 5).

Heat waves' definition in three-dimensional (3D) space

Separately for each region, a two-dimensional (longitude–latitude) matrix containing values of the 95th percentile of T2M for summer (June–August) was calculated in the first step. T2M anomalies from the 95th percentile were then obtained for each day and grid box in the 1979–2022 period. To achieve 3D insight into heat waves' temperature structure, an analogous procedure was performed at all 12 levels between 850 and 300 hPa. Daily mean T2M was adopted instead of daily maximum temperature (which is commonly used for conventional 2D heat waves' definitions in near-surface data) due to small diurnal temperature variations higher in the troposphere. In the next step, for each level and day separately, the spatial information of temperature anomalies was transformed into one-dimensional characteristics: (i) area of positive temperature anomalies above the 95th percentile (A;

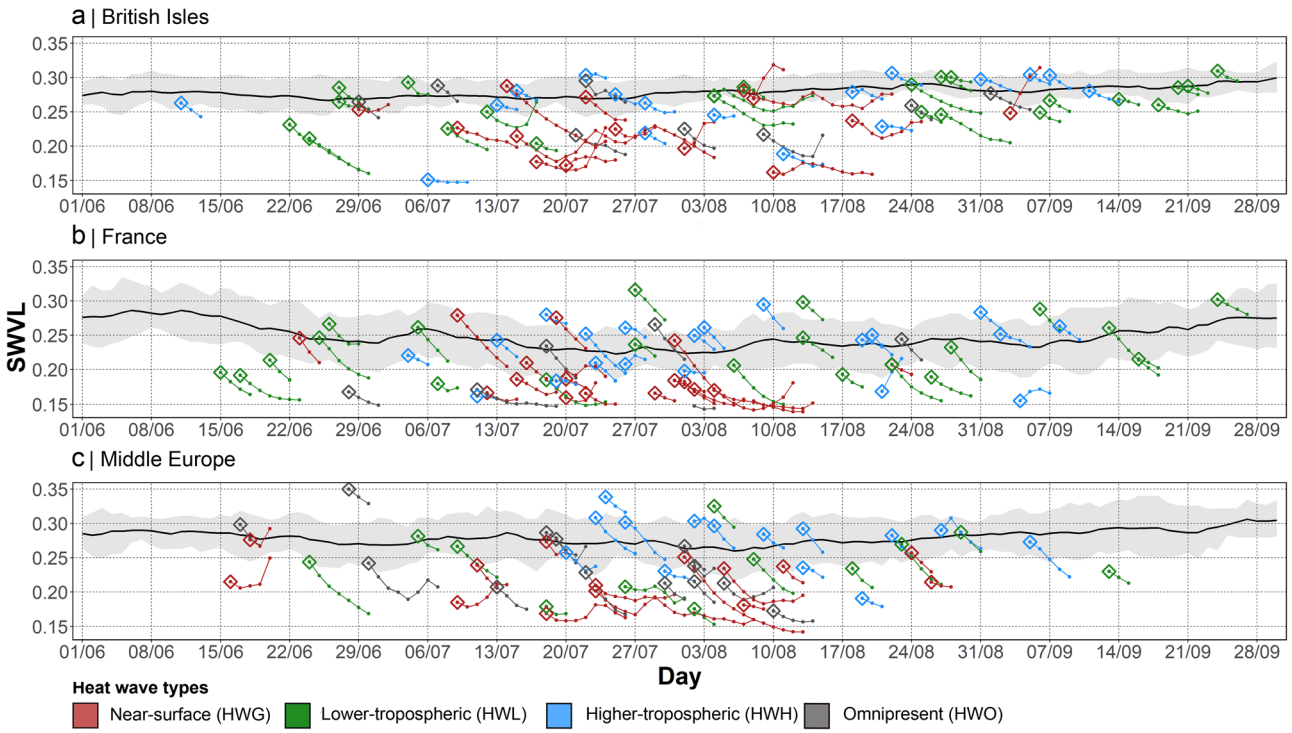

Fig. 4 | Development of soil moisture during individual heat waves. Temporal evolution of near-surface (0–7 cm depth) volumetric soil water (SWVL) during individual heat waves in **a** the British Isles, **b** France, and **c** Middle Europe. Highlighted points indicate the starting days of heat waves. The black line represents the 1991–2020 climatological mean of volumetric soil water for a given day and the gray band its interquartile range.

Table 2 | Characteristics of soil moisture prior to and during heat waves

	British Isles				France				Middle Europe			
	HWG	HWL	HWH	HWO	HWG	HWL	HWH	HWO	HWG	HWL	HWH	HWO
Start	0.230*	0.266	0.262	0.255	0.197*	0.235	0.232	0.205	0.225*	0.246*	0.277	0.247*
End	0.232	0.246	0.250	0.236	0.175	0.201	0.218	0.176	0.211	0.212	0.249	0.221
Diff	−0.002	0.020	0.012	0.020	0.023	0.034	0.014	0.029	0.014	0.033	0.028	0.026
14D	0.251*	0.285	0.269	0.243	0.222*	0.256	0.239	0.245	0.253*	0.278	0.280	0.257
Clim	0.278				0.254				0.284			

Soil moisture content (SWVL) in the analysed regions. "Start (End)" indicates the mean soil moisture content for the first (last) day of heat waves, and "Diff" stands for the mean difference in SWVL between the first and last days of heat waves. "14D" represents the mean SWVL in the period 14 days long prior to heat waves. "Clim" is the mean June–September SWVL in 1991–2020. "*" denotes significantly (at 1% level) lower SWVL in the first days or in the period 14 days prior to heat waves compared to its climatology for the June–September period.

[proportion of the region]) and (ii) mean value of positive temperature anomalies (T; [°C]).

For a straightforward interpretation of heat waves' 3D structures, the 6 lower levels (850–600 hPa) were aggregated (area and mean positive anomalies were averaged for each day) into one layer (lower troposphere; LO), while the remaining 6 higher (550–300 hPa) levels were merged into the higher troposphere (HI). The boundary between LO and HI set between 600 and 550 hPa corresponds to the maximum depth of the atmospheric boundary layer during major heat waves[10]. T2M was preserved as a separate near-surface layer (NS, also to allow comparison with conventional definitions of 2D heat waves). A heat wave is defined as a sequence of at least 3 consecutive days when an area of positive temperature anomalies above the 95th percentile was larger than one-third of the region in any layer (NS, LO, or HI). In cases of two heat waves separated by 1 or 2 days only, these were merged into one event, similar to ref. 32.

Extremity of heat waves and their typology

The methodology allows heat waves to occur anywhere in the (almost entire) troposphere. To distinguish between heat wave types, their extremity ("E") in each layer was calculated as follows:

$$\begin{aligned} E_{NS} &= \overline{T_{NS}} \times \overline{A_{NS}} \times L \\ E_{LO} &= \overline{T_{LO}} \times \overline{A_{LO}} \times L \\ E_{HI} &= \overline{T_{HI}} \times \overline{A_{HI}} \times L \end{aligned} \quad (1)$$

where "T" stands for daily mean values of positive temperature anomalies above the 95th percentile, averaged over all days during which a heat wave persists; "A" represents the area of positive temperature anomalies given as a proportion of the region, analogously averaged across all heat wave days; and "L" is the length of a heat wave in days. NS, LO, and HI subscripts indicate individual layers. The extremity, therefore, represents the joint effects of the heat wave's positive temperature anomalies, spatial extent, and length. The overall extremity (E_{ALL}) of heat waves is calculated as a sum over individual layers:

$$E_{ALL} = E_{NS} + E_{LO} + E_{HI} \quad (2)$$

Heat waves were classified into four types, indicating their predominant vertical location. Near-surface (HWG), lower-tropospheric (HWL), higher-tropospheric (HWH), and omnipresent (HWO) heat waves were defined based on their extremity in individual layers:

$$\begin{aligned} &if\ \frac{E_{NS}}{E_{ALL}} > 0.5 \rightarrow HWG \\ &if\ \frac{E_{LO}}{E_{ALL}} > 0.5 \rightarrow HWL \\ &if\ \frac{E_{HI}}{E_{ALL}} > 0.5 \rightarrow HWH \\ &otherwise \rightarrow HWO \end{aligned} \quad (3)$$

Statistical testing

The statistical significance of soil moisture preconditioning was assessed using the non-parametric Wilcoxon test (assumptions for the *t*-test were not always met). Regionally averaged daily SWVL values for (i) the first days of heat waves and (ii) periods of 14 days prior to their onset were compared to the mean SWVL value for the June–August period in 1991–2020.

Data availability

The ERA5 data can be downloaded from the Copernicus Climate Data Store[46,47]. Figure source data are available in the Mendeley data repository[48].

Received: 1 February 2024; Accepted: 6 June 2024;
Published online: 14 June 2024

References

1. Marx, W., Haunschild, R. & Bornmann, L. Heat waves: a hot topic in climate change research. *Theor. Appl. Climatol.* **146**, 781–800 (2021).
2. Lu, R. et al. Heat waves in summer 2022 and increasing concern regarding heat waves in general. *Atmos. Ocean. Sci.* **16**, 100290 (2023).
3. Henderson, S. B. et al. Analysis of community deaths during the catastrophic 2021 heat dome: early evidence to inform the public health response during subsequent events in greater Vancouver, Canada. *Environ. Epidemiol.* **6**, e189 (2022).
4. White, R. H. et al. The unprecedented Pacific Northwest heatwave of June 2021. *Nat. Commun.* **14**, 727 (2023).
5. Jiang, J. et al. Extreme heatwave over Eastern China in summer 2022: the role of three oceans and local soil moisture feedback. *Environ. Res. Lett.* **18**, 044025 (2023).
6. Yule, E. L. et al. Using early extremes to place the 2022 UK heat waves into historical context. *Atmos. Sci. Lett.* **24**, e1159 (2023).
7. Barriopedro, D. et al. Heat waves: physical understanding and scientific challenges. *Rev. Geophys.* **61**, e2022RG000780 (2023).
8. Barriopedro, D. et al. The hot summer of 2010: redrawing the temperature record map of Europe. *Science* **332**, 220–224 (2011).
9. Lokoshchenko, M. A. et al. Air temperature in the lower troposphere over Moscow during heat wave in the summer of 2010. *Atmos. Ocean. Opt.* **29**, 267–273 (2016).
10. Miralles, D. G. et al. Mega-heatwave temperatures due to combined soil desiccation and atmospheric heat accumulation. *Nat. Geosci.* **7**, 345–349 (2014).
11. Fischer, E. Autopsy of two mega-heatwaves. *Nat. Geosci.* **7**, 332–333 (2014).
12. Zhang, Y. et al. Aircraft observed diurnal variations of the planetary boundary layer under heat waves. *Atmos. Res.* **235**, 104801 (2020).
13. Santanello, J. A., Friedl, M. A. & Ek, M. B. Convective planetary boundary layer interactions with the land surface at diurnal time scales: diagnostics and feedbacks. *J. Hydrometeor.* **8**, 1082–1097 (2007).
14. Seneviratne, S. I. et al. Investigating soil moisture–climate interactions in a changing climate: a review. *Earth Sci. Rev.* **99**, 125–161 (2010).
15. Schumacher, D. L. et al. Amplification of mega-heatwaves through heat torrents fuelled by upwind drought. *Nat. Geosci.* **12**, 712–717 (2019).
16. Benson, D. O. & Dirmeyer, P. A. Characterizing the relationship between temperature and soil moisture extremes. *J. Clim.* **34**, 2175–2187 (2021).
17. Stéfanon et al. Soil moisture-temperature feedbacks at meso-scale during summer heat waves over Western Europe. *Clim. Dyn.* **42**, 1309–1324 (2013).
18. Lansu, E. M. et al. Atmospheric aridity and apparent soil moisture drought in European forest during heat waves. *Geophys. Res. Lett.* **47**, e2020GL087091 (2020).
19. Hersbach, H. et al. The ERA5 global reanalysis. *Q. J. Roy. Meteor. Soc.* **146**, 1999–2049 (2020).
20. Christensen, J. H. & Christensen, O. B. A summary of the PRUDENCE model projections of changes in European climate by the end of this century. *Clim. Change* **81**, 7–30 (2007).
21. Vautard, R. et al. Evaluation of the large EURO-CORDEX regional climate model ensemble. *J. Geophys. Res. Atmos.* **126**, e2019JD032344 (2021).
22. Manning, C. et al. Soil moisture drought in Europe: a compound event of precipitation and potential evapotranspiration on multiple time scales. *J. Hydrometeor.* **19**, 1255–1271 (2018).
23. Vautard, R. et al. Human contribution to the record-breaking June and July 2019 heatwaves in Western Europe. *Environ. Res. Lett.* **15**, 094077 (2020).
24. Zschenderlein et al. Processes determining heat waves across different European climates. *Q. J. R. Meteorol. Soc.* **145**, 2973–2989 (2019).
25. Holmberg, E. et al. The link between European warm-temperature extremes and atmospheric persistence. *Earth Syst. Dynam.* **14**, 737–765 (2023).
26. de Villiers, M. P. Europe extreme heat 22–26 July 2019: was it caused by subsidence or advection? *Weather* **75**, 228–235 (2020).
27. Domeisen, D. I. et al. Prediction and projection of heatwaves. *Nat. Rev. Earth Environ.* **4**, 36–50 (2023).
28. Röthlisberger, M. & Papritz, L. Quantifying the physical processes leading to atmospheric hot extremes at a global scale. *Nat. Geosci.* **16**, 210–216 (2023).
29. Beniston, M. The 2003 heat wave in Europe: a shape of things to come? An analysis based on Swiss climatological data and model simulations. *Geophys. Res. Lett.* **31**, L02202 (2004).
30. Zschenderlein et al. Large-scale Rossby wave and synoptic-scale dynamic analyses of the unusually late 2016 heatwave over Europe. *Weather* **73**, 275–283 (2018).
31. Ballester, J. et al. Heat-related mortality in Europe during the summer of 2022. *Nat. Med.* **29**, 1857–1866 (2023).
32. Lhotka, O. & Kyselý, J. The 2021 European heat wave in the context of past major heat waves. *Earth Space. Sci.* **9**, e2022EA002567 (2022).
33. Kendon, M. et al. State of the UK Climate 2022. *Int. J. Climatol.* **43**, 1–82 (2023).
34. Ionita, M. & Nagavciuc, V. Changes in drought features at the European level over the last 120 years. *Nat. Hazard Earth Sys. Sci.* **21**, 1685–1701 (2021).
35. Stegehuis, A. I. et al. Early summer soil moisture contribution to Western European summer warming. *J. Geophys. Res. Atmos.* **126**, e2021JD034646 (2021).
36. Palarz, A., Celiński-Mysław, D. & Ustrnul, Z. Temporal and spatial variability of elevated inversions over Europe based on ERA-Interim reanalysis. *Int. J. Climatol.* **40**, 1335–1347 (2020).
37. Horton, D. et al. Contribution of changes in atmospheric circulation patterns to extreme temperature trends. *Nature* **522**, 465–469 (2015).
38. Sousa, P. M. et al. European temperature responses to blocking and ridge regional patterns. *Clim. Dyn.* **50**, 457–477 (2018).

39. Kautz, L.-A. et al. Atmospheric blocking and weather extremes over the Euro-Atlantic sector – a review. *Weather Clim. Dynam.* **3**, 305–336 (2022).
40. Chiriaco, M. S. et al. European heatwave in July 2006: observations and modeling showing how local processes amplify conducive large-scale conditions. *Geophys. Res. Lett.* **41**, 5644–5652 (2014).
41. Liu, X. et al. Similarities and differences in the mechanisms causing the European summer heatwaves in 2003, 2010, and 2018. *Earth's Future* **8**, e2019EF001386 (2020).
42. Lavers, D. A. et al. An evaluation of ERA5 precipitation for climate monitoring. *Q. J. R. Meteorol. Soc.* **148**, 3124–3137 (2022).
43. Lhotka, O. & Kyselý, J. Precipitation–temperature relationships over Europe in CORDEX regional climate models. *Int. J. Climatol.* **42**, 4868–4880 (2022).
44. Cornes, R. C. et al. An ensemble version of the E-OBS temperature and precipitation data sets. *J. Geophys. Res. Atmos.* **123**, 9391–9409 (2018).
45. Miralles, D. G. et al. Land–atmospheric feedbacks during droughts and heatwaves: state of the science and current challenges. *Ann. N.Y. Acad. Sci.* **1436**, 19–35 (2019).
46. ECMWF. ERA5 hourly data on single levels from 1940 to present [Dataset]. *Copernicus Climate Change Service* (*C3S*) *Climate Data Store* (*CDS*). https://doi.org/10.24381/cds.adbb2d47 (2023).
47. ECMWF. ERA5 hourly data on pressure levels from 1940 to present [Dataset]. *Copernicus Climate Change Service* (*C3S*) *Climate Data Store* (*CDS*). https://doi.org/10.24381/cds.bd0915c6 (2023).
48. Lhotka, O. & Kyselý, J. Figure source files for article three-dimensional analysis reveals diverse heat wave types in Europe, *Mendeley Data*, V1. https://doi.org/10.17632/fkfywnjcr8.1 (2024).

Acknowledgements

The study was supported by the Czech Science Foundation, project 23-06749S. We acknowledge the ERA5 reanalysis from the European Centre for Medium-Range Weather Forecasts (ECMWF).

Author contributions

O.L. Conceptualization, methodology, formal analysis, visualization, writing original draft and revised manuscript, funding acquisition. J.K. Supervision, validation, writing original draft and revised manuscript, funding acquisition.

Competing interests

The authors declare no competing interests.

Additional information

Supplementary information The online version contains supplementary material available at https://doi.org/10.1038/s43247-024-01497-2.

Correspondence and requests for materials should be addressed to Ondřej Lhotka.

Peer review information *Communications Earth & Environment* thanks the anonymous reviewers for their contribution to the peer review of this work. Primary Handling Editors: Alireza Bahadori and Aliénor Lavergne. A peer review file is available.